(to appear in the Astronomical Journal)

# The Universality of the Fundamental Plane of E and S0 Galaxies. Sample Definition and I Band Photometric Data

Marco Scodeggio[1,2], Riccardo Giovanelli[1] and Martha P. Haynes
Center for Radiophysics and Space Research and National Astronomy and Ionosphere Center[3],
Cornell University, Ithaca, NY 14853
mscodegg@eso.org
riccardo, haynes@astrosun.tn.cornell.edu

## ABSTRACT

As part of a project to compare the Fundamental Plane and Tully-Fisher distance-scales, we present here I band CCD photometry for 636 early-type galaxies in 8 clusters and groups of galaxies. These are the A262, A1367, Coma (A1656), A2634, Cancer and Pegasus clusters, and the NGC 383 and NGC 507 groups. Sample selection, cluster properties, and cluster membership assignment criteria are discussed. We present photometric parameters that are used in the Fundamental Plane relation, the effective radius $r_e$ and the effective surface brightness $\mu_e$, as derived from a $r^{1/4}$ fit to the observed radial photometric profile of each galaxy. A comparison with similar data found in the literature for the Coma cluster shows that large systematic uncertainties can be introduced in the measurement of $r_e$ and $\mu_e$ by the particular method used to derive those parameters. However the particular combination of these two parameters that enters in the Fundamental Plane relation is a quantity that can be measured with high accuracy.

*Subject headings:* distance scale — galaxies: distances and redshifts — galaxies: elliptical and lenticular — galaxies: fundamental parameters — galaxies: photometry

---

[1]Visiting Astronomer, Kitt Peak National Observatory, National Optical Astronomy Observatories, which is operated by the Association of Universities for Research in Astronomy, Inc. (AURA) under cooperative agreement with the National Science Foundation.

[2]Present address: European Southern Observatory, Karl-Schwarzschild-Straße 2, D-85748, Garching bei München, Germany.

[3]The National Astronomy and Ionosphere Center is operated by Cornell University under a cooperative agreement with the National Science Foundation.

## 1. Introduction

This is the third in a series of papers (Scodeggio, Giovanelli & Haynes 1997a,b; hereafter Paper I and Paper II) devoted to a study of the universality of the Fundamental Plane (FP) relation of early-type galaxies (Djorgovski & Davis 1987; Dressler *et al.* 1987). This relation, and the equivalent Tully-Fisher (TF) relation for spiral galaxies (Tully & Fisher 1977), have been widely used in the recent past to produce large samples of redshift-independent distance estimates. The small scatter of the FP relation has been also used to put constraints on the epoch of early-type galaxy formation, and on the subsequent evolution and star formation histories of those objects (see for example Guzmàn, Lucey & Bower 1993; Renzini & Ciotti 1993; van Dokkum & Franx 1996; Pahre & Djorgovski 1997).

Both applications are based on the assumption that the FP and TF relations are universal: all galaxies in all locations and environments have effective radius, effective surface brightness and velocity dispersion, or magnitude and rotation velocity that are related by the same relation, within measurement uncertainties and the intrinsic dispersion present in the relations. However, this might not be the case, since a number of environmental effects are known to exist that have the potential of altering significantly the stellar population and star formation history of the affected galaxies. Therefore, the FP and TF universality should not be taken for granted, but should rather be observationally verified (discussions on this subject are presented by Djorgovski, de Carvalho & Han 1988; Guzmán *et al.* 1992; Jørgensen, Franx & Kjærgaard 1996; Schroeder 1996; Giovanelli *et al.* 1997b; and in Paper I).

The most direct way to test the reliability of a distance indicator relation is to compare its predictions with those of another independent, and at least equally reliable, method. The TF and FP relations provide the opportunity for such a comparison. They have similar accuracy, and they are independent methods, because they are applied to galaxies of different morphological type and different clustering properties. Because of the limited accuracy of the distance estimates obtained with the TF and FP relation, a direct comparison of the two methods can be done most effectively using clusters of galaxies, where large samples can be used to reduce the statistical uncertainty in the estimate of the cluster distances. It should be kept in mind, however, that given the existing correlation between cluster richness and the properties of the intracluster medium (see for example Edge & Stewart 1991), it is desirable that such a comparison bridge a set of clusters characterized by a wide range of richness, in order for the TF-FP comparison to have broad validity.

In a recent work, Giovanelli *et al.* (1997a,b; hereafter G97a,b) have presented TF measurements for a large sample of cluster objects. This represent the largest dataset currently available that can be used for estimating cluster distances using the TF relation. In this and the following papers of this series, we present the results of a FP study of a subset (eight clusters) of the clusters studied by G97a,b. The main purpose of this work is to obtain distance estimates for those clusters, with accuracies comparable to those achievable using the TF dataset, to be used for a comparison between the two methods. In this paper, we briefly describe the cluster sample selection and the adopted cluster membership criteria, and we present I band CCD photometry for 636 early-type galaxies in those clusters. In a companion paper (Scodeggio, Giovanelli & Haynes 1998a), we present the results of spectroscopic observations of a subset of these galaxies. Following that work, we will discuss the properties of the I band FP relation, and the comparison between TF and FP distance estimates for the clusters in our sample (Scodeggio, Giovanelli & Haynes 1998b).

The cluster sample selection is described in Section 2; observations and the data reduction procedure are described in Section 3 and 4; the photometric sample is presented in Section 5. An assesment of the quality of the photometric data presented in this work is presented in Section 6. Throughout the paper we parametrize distance–dependent quantities via $H_\circ = 100h$ km s$^{-1}$Mpc$^{-1}$ .

## 2. Cluster sample selection and membership

Recently G97a,b have presented TF measurements for a sample of $\simeq$ 800 galaxies in 24 clusters. Because one of the goals of that work was to obtain a kinematical rest frame that could be used to study the local peculiar velocity field, it was important that such sample of clusters had a rather uniform sky coverage, so that localized anomalies in the velocity field would average out in the global sample. On the contrary, the main goal of this work is a detailed, point-by-point comparison of distance estimates, irrespective of the possible peculiar velocities that the target clusters might have. Therefore a uniform sky coverage is not an important requirement for our sample. It is essential instead to cover a wide spread in cluster richness and the properties of the intracluster medium (ICM), since known environmental effects on galaxies are strongly dependent on the local galaxy density, or on the density of the ICM. We have therefore selected a subset of the clusters in G97a,b as targets for the FP study, restricted to the northern hemisphere, mainly to facilitate the spectroscopic observations. The set is composed of the 8 clusters and rich groups of galaxies NGC 383 group, NGC 507 group, A262, Cancer, A1367, Coma (A1656), Pegasus, A2634.

### 2.1. Cluster properties

Table 1 lists the most important properties of these clusters and groups. The cluster center is generally assumed to be coincident with the position of the brightest galaxy, except in the case of the irregular cluster A1367, where the center is assumed to be at the mid-point between the two brightest ellipticals. Systemic heliocentric velocity and velocity dispersion are taken from the literature, according to the references quoted in the table. Heliocentric velocities are converted to the cosmic microwave background (CMB) reference frame using the CMB dipole determintion from Kogut *et al.* (1993). Population fractions data are from Dressler (1980), and Giovanelli & Haynes (1985), while the fraction of HI deficient objects in a cluster (this is the fraction of spiral galaxies that have HI deficiency $> 0.3$, according to the definition of Giovanelli & Haynes 1985 and Haynes & Giovanelli 1984) is taken from Giovanelli & Haynes (1985), and Magri *et al.* (1988). X-ray data are taken from David *et al.* (1993).

The most extreme properties within our sample are those of the Coma cluster, a rich, dynamically relaxed, and X-ray luminous cluster, that exhibits strong morphological segregation and HI deficiency among the spiral galaxy population. Then we have medium richness clusters like A2634 and A1367: the first is a dynamically evolved cluster (see however Pinkney *et al.* 1993 and Schindler & Prieto 1997 for a discussion on a possible recent merger event in A2634), exhibiting clear morphological segregation and pronounced HI deficiency among the spiral galaxy population, while the second is an irregular cluster, with only moderate morphological segregation and HI deficiency. A262 is a transitional cluster, where low X-ray luminosity and velocity dispersion, cool ICM temperature, and high spiral fraction, all indicative of a dynamically unevolved state, coexist with the presence of a massive dominant galaxy, which is typical of more evolved systems (see for example Forman & Jones 1982, and Sarazin 1988). The cluster exhibits moderate morphological segregation and HI deficiency. The low end of the cluster richness distribution is represented by the Pegasus and Cancer clusters. Both are spiral rich, low X-ray luminosity objects, that exhibit little morphological segregation and marginal HI deficiency. Here we refer to Cancer as the largest of the separate groups that were identified by Bothun *et al.* (1983) over the area and redshift range traditionally associated with the Cancer cluster. This is group A in the nomenclature of Bothun *et al.* The rich groups associated with the galaxies NGC 507 and NGC 383 are often considered as a single entity, the so-called Pisces cluster. However Sakai, Giovanelli & Wegner (1994) have clearly shown that the two can be separated. In both groups the galaxy population is dominated by elliptical and S0 galaxies, and HI deficiency is almost absent among the spiral galaxy population.

### 2.2. Cluster membership

A discussion of the membership criteria adopted for the TF work on the clusters in the present sample was presented by G97a (their section 8). Here we adopt the same basic criteria, with the advantage that the bulk of the early-type galaxy population is concentrated towards the cluster centers, where the application of those criteria is easier than at the cluster periphery. Therefore we do not separate our FP sample into certain and possible cluster members, as done in G97a,b, but we define only *bona-fide* cluster members. The photometric sample presented here, however, includes also a number of galaxies for which spectroscopic data is not available, considered likely cluster members on the basis of their size and I band flux.

Whenever caustic lines in redshift space (Kaiser 1987, Regös & Geller 1989, van Haarlem 1992) are available for one of the clusters in our sample, membership determination is based on those lines, as estimated for $\Omega_\circ = 0.3$. This is the case for Coma, where caustic lines have been published by Regös & Geller (1989), van Haarlem (1992), and Gavazzi, Randone & Branchini (1995); A2634, where they have been published by Scodeggio et al. (1995); and A1367, where they have been published by Regös & Geller (1989), and Gavazzi *et al.* (1995). For Coma and A1367 we use the caustic lines published by Regös & Geller (1989).

For A262, we use the detailed analysis of the spatial and velocity distribution of the galaxies in the A262 area presented by Sakai *et al.* (1994). Although they did not derive redshift space caustic lines for this cluster, their work can be used to derive reliable membership criteria, out to a radial distance of 2° from the cluster center, beyond which the contamination from the sparse population of the Perseus-Pisces Supercluster becomes significant. We define as A262 members all galaxies within 2° from the cluster center, with $cz_{hel}$ within the interval 3500–6300 km s$^{-1}$. Pegasus is well separated in redshift space from foreground and background objects, and membership assignments are not problematic, especially for the early-type population. We define as Pegasus members all galaxies within 2° from the cluster center, with $cz_{hel}$ within the interval 2700–5100 km s$^{-1}$. For Cancer, we use the membership table published by Bothun *et al.* (1983) for group A. For the NGC 383 and NGC 507 groups, we use the analysis published by Sakai *et al.* (1994). Although redshift space caustic lines could not be reliably derived, because of the small samples involved, membership can be assigned confidently, thanks to the relative under-density of the region in front and behind the two groups. Here we define as NGC 507 members all galaxies within 1.5° from the group center, with $cz_{hel}$ within the interval 3500–6700 km s$^{-1}$, and as NGC 383 members all galaxies within 1.0° from the group center, with $cz_{hel}$ within the interval 3800–6500 km s$^{-1}$.

## 3. Observations

All photometric measurement have been derived from I-band CCD images. The adoption of I band for photometry was mainly dictated by the practical notion that the cluster images contain several galaxies per frame, both of early- and late-type, and thus can be useful for TF application, where the I band is favored for compatibility with G97a,b.

Most of the observations were obtained during three runs with the 0.9m telescope of the Kitt Peak National Observatory (KPNO). A small number of observations in the cluster A2634 was obtained during observing runs with the 1.3m telescope of the Michigan-Dartmouth-MIT (MDM) Observatory (runs 1 and 3 in Table 2). Other observations in A2634 were obtained by KPNO staff with the 0.9m telescope during a period of service observations (run 2 in Table 2). Table 2 lists all observing runs during which data were obtained for this project, and gives parameters of the instrumental setups. The most significant difference between the MDM and the KPNO observations is the much smaller field of view of the 1.3m MDM telescope, when compared with the 0.9m KPNO telescope.

All CCD frames were obtained with 600 seconds integration time. For the brightest objects, a second frame with shorter integration (200–300 seconds) was necessary to avoid saturation of the image in the nuclear region of the galaxy. The median effective seeing (measured as the FWHM of the stellar light profile) for the entire data set is 1.6". Figure 1 shows the distribution of effective seeing for the galaxy observations. The actual atmospheric seeing might have been smaller at times, but the pixel size with which the majority of the observations were obtained limits the effective seeing to $\geq$1.2". Given the large field of view of the KPNO 0.9m telescope, and the large density of galaxies in the cluster environments studied here, a complete mapping of the clusters' central regions was obtained, with a mosaic of frames on a regularly spaced grid. Only for the galaxies at the periphery of the various clusters off-grid pointings were used.

## 4. Data reduction

### 4.1. Basic reduction

The data reduction process was performed entirely using a combination of standard and specially written IRAF[4] procedures. All frames were bias-subtracted, and flat-fielded using a "superflat" obtained from a median-filtered combination of a large (n>40) number of frames. At this point, for ease of manipulation, one small frame (512 x 512 pixels) for each target galaxy was extracted from the 2048 x 2048 KPNO pixel frames. The 1024 x 1024 pixel MDM frames were kept as single frames. The sky background was subtracted from all frames, using the average number of counts measured in 10–12 "empty-sky"' regions. The typical number of pixels over which this average was computed is 30,000. The accuracy of the background determination can be estimated from the comparison of the independent values subtracted from different 512 x 512 pixel frames extracted from the same $2048 \times 2048$ pixel frame. This uncertainty is typically of 0.2%. All pixels contaminated by the light of foreground stars or other galaxies, or by cosmic rays hits were blanked and excluded from the final steps of surface photometry.

For galaxies severely contaminated by the light of a nearby object (either another galaxy or a foreground star), an iterative subtraction procedure was used to obtain the individual light profiles. First, a model was fitted to the brighter object, after blanking the fainter one(s). After subtracting such model from the original image, a model was fitted to the fainter object, which again was subtracted from the original image. The procedure was iteratively applied until convergence was reached, usually at the second iteration, producing companion-subtracted light profiles, although the uncertainty on the photometry of these objects is somewhat higher than for isolated galaxies. This approach is especially necessary in the inner parts of clusters, where the galaxy density is high.

### 4.2. Photometric calibration

One or two Landolt (1992) fields, containing each one from 5 to 7 stars, were repeatedly observed during each night, at airmasses between 1.2 and 2.5, to provide estimates of the

[4]IRAF (Image Reduction and Analysis Facility) is distributed by the National Optical Astronomy Observatories.

photometric zero-point and atmospheric extinction coefficient. Observations at I and R band were used to obtain color corrected photometric solutions. Typical uncertainties in the zero-point determination are 0.02 mag, both at I and R band. All galaxy magnitudes were computed assuming a constant R–I color of 0.70 for elliptical, S0, and S0a galaxies (see, for example, Fukugita, Shimasaku & Ichikawa 1995). The uncertainty introduced by this assumption is negligible, because the color term coefficient is always very small ($< 0.05$). Galaxy observations were all obtained at airmass $< 1.3$, thereby minimizing the effects of atmospheric extinction.

Most observations were obtained in photometric conditions. Those that were not were calibrated using either short exposure frames obtained in photometric conditions (run 2 was calibrated entirely in this way, using frames obtained during run 3), or taking advantage of the partial overlap among frames in the mapping grid (non photometric nights in runs 4, 5, 7, 8 were calibrated using this technique). In either case 10–15 stars that are present in both the "photometric" and the "non photometric" image were selected, and instrumental (i.e. non calibrated) magnitudes for all them were obtained in both images. After rejecting the obvious variable stars, mean magnitude differences between the stars in the two images were used to calibrate the "non photometric" frames. The typical uncertainty of this process is $\simeq$0.03 mag.

### 4.3. Surface photometry

Surface photometry was obtained using the GALPHOT software package, written for IRAF/STSDAS[5] mainly by W. Freudling, J. Salzer and M. Haynes. A galaxy's light distribution was fitted with elliptical isophotes, using a modified version of the STSDAS *Isophote* package. The center, ellipticity and position angle of the ellipse were free parameters, while the ellipse semi-major axis was incremented by a fixed fraction of its value at each step of the fitting procedure. The procedure was stopped when the fitted mean number of counts per pixel dropped below the rms dispersion around the mean value. For this dataset, this typically happens close to the 23.5 mag arcsec$^{-2}$ isophote. The fitted parameters yielded a model of the galaxy, which was used to compute integrated magnitudes as a function of semi-major axis. At this point the measured fluxes in counts per pixel were transformed into magnitudes per square arcsec, and all magnitudes were calibrated, color-corrected, and corrected for atmospheric extinction.

The radial surface brightness profiles were fitted with a $r^{1/4}$ profile (de Vaucouleurs 1948), to determine the effective radius $r_e$ (the radius that contains half of the galaxy total light) and the effective surface brightness $\mu_e$ (the mean surface brightness within the effective radius). For all galaxies, the fit was performed from an inner radius twice as large as the seeing disk radius of the relative image. The outer radius was chosen depending on the shape of the surface brightness

[5]STSDAS (Space Telescope Science Data Analysis System) is distributed by the Space Telescope Science Institute, which is operated by AURA, under contract to the National Aeronautics and Space Administration.

profile. For those objects that are well described by the $r^{1/4}$ law at all radii, the fit was extended to the outermost isophotes. For all other galaxies, only the central core was fitted. The effective radius $r_e$ and the surface brightness at $r_e$ were the two free parameters in the fit, and the effective surface brightness $\mu_e$ was obtained from $\mu(r_e)$ as $\mu_e = \mu(r_e) - 1.392$ (this is strictly valid only for a galaxy that follows the $r^{1/4}$ profile at all radii). The median value for the uncertainty of the fits is 6.2% in $r_e$, and 0.07 mag arcsec$^{-2}$ in $\mu_e$.

Integrated fluxes within the faintest reliably measured isophote were obtained. Total magnitudes were derived from those, by adding a term which was obtained by extrapolating the surface brightness profile to infinity. For those galaxies not well represented by the $r^{1/4}$ law at all radii the outer portion of the profile was fitted using either a different $r^{1/4}$ profile from the one used to fit the core of the galaxy, or an exponential disk profile, depending on the profile shape. The median uncertainty with which total magnitudes were derived is 0.06 mag.

Total magnitudes and effective surface brightnesses were corrected for Galactic extinction and cosmological effects. Extinction corrections were computed for each galaxy following the prescriptions of Burstein & Heiles (1978), using $A_I = 0.45 A_V$. These corrections range from 0.0 to 0.13 mag. Statistically equivalent results are obtained using the extinction maps recently published by Schlegel, Finkbeiner & Davis (1998). Cosmological K-corrections were computed assuming $F_\nu \sim \nu^0$ (the energy distribution of early-type galaxies in the red is nearly flat) so that $K_I = 2.5 \log(1 + z)$, and range from 0.01 to 0.04 mag. The $(1+z)^4$ cosmological corrections to surface brightness range from 0.04 to 0.15 mag arcsec$^{-2}$. Effective radius and effective surface brightness were corrected for the smearing effects of seeing, following the prescriptions of Saglia *et al.* (1993a, see in particular their Figure 8). The seeing correction produced a median reduction of 2% of the measured values of $r_e$, and a median correction of 0.016 mag arcsec$^{-2}$ to the measured values of $\mu_e$.

## 5. The photometric sample

In each cluster, surface photometry was obtained for E, S0, and S0a galaxies, potentially good candidates for FP work. A few galaxies that were classified as S0a/Sa or Sa were included in the sample because a velocity dispersion measurement was already available for them. Known foreground or background objects were excluded, while a number of galaxies without redshift measurement, but with flux and size that make them likely cluster members, were instead included in the samples, except in the case of the Cancer cluster, where foreground and background contamination is too pronounced. Galaxies in close pairs or multiplets, and galaxies contaminated by bright foreground stars projected over the galaxy or in its immediate vicinity were rejected, unless a velocity dispersion measurement was already available. Only in these cases was an attempt made to subtract the contribution of the contaminating object to the observed light distribution (see section 4.1). In total, photometric properties for 636 galaxies were measured. The final samples are close to magnitude-limited in nature, as will be seen in the discussion on the

FP relation (Scodeggio *et al.* 1998b; see also the discussion in Paper II).

The photometric data are presented in Table 3. Only the first page of this table is presented here for guidance regarding its form and content; the entire table is available in digital form on the Journal Electronic Edition, or from the authors. The table is organized as follows:
Col. 1: Galaxy name: if the galaxy is listed in the UGC catalog (Nilson 1973), the UGC number is given; if not, our internal coding number, from the private galaxy catalog of Giovanelli & Haynes referred to as the AGC, is given.
Cols. 2 and 3: the NGC or IC number, if available, and the CGCG field and ordinal number within that field, if the galaxy is listed in the CGCG (Zwicky *et al.* 1963-1968). For galaxies in the Coma cluster that are not listed in either one of those catalogs, the Dressler number (Dressler 1980) is given, if available.
Cols. 4 and 5: Right Ascension and Declination, in 1950.0 epoch.
Col. 6: morphological type code, in the RC3 (de Vaucouleurs *et al.* 1991) scheme (-5 for E, -2 for S0, 0 for S0a). Morphological types were derived from joint inspection of the blue plates of the Palomar Observatory Sky Survey (POSS), and of the CCD images.
Col. 7: Heliocentric radial velocity $V_{hel}$, in $\mathrm{km\,s^{-1}}$.
Col. 8: Measured effective radius $r_e$, in arcsec.
Col. 9: Effective radius corrected for seeing effects $r_e^c$, in arcsec.
Col. 10: Uncertainty on the effective radius $\epsilon_r$, in arcsec.
Col. 11: Corrected metric effective radius $R_e$, in kiloparsec, obtained assuming the galaxy is at the distance indicated by the cluster redshift, in the CMB reference frame.
Col. 12: Measured effective surface brightness $\mu_e$, in I band mag arcsec$^{-2}$.
Col. 13: Corrected effective surface brightness $\mu_e^c$, in I band mag arcsec$^{-2}$. $\mu_e^c$ is corrected for the smearing effects of seeing, for extinction within our Galaxy, for the cosmological k-correction term, and for $(1+z)^4$ cosmological dimming.
Col. 14: Uncertainty on the effective surface brightness $\epsilon_\mu$, in mag arcsec$^{-2}$.
Col. 15: Measured apparent I band magnitude $m_I$, obtained extrapolating the surface brightness profile to infinity.
Col. 16: Corrected apparent I band magnitude $m_I^c$, obtained from the value listed in col. 15, and corrected for extinction within our Galaxy, and for the cosmological k-correction term. No internal extinction correction was applied.
Col. 17: Uncertainty on the measured magnitude, $\epsilon_m$.
Col. 18: Absolute magnitude $M_I$, obtained assuming that the galaxy is at the distance indicated by the cluster redshift, in the CMB reference frame.
Col. 19: Quality codes, as follows:
First digit = Photometric code: 1 = observation obtained in photometric conditions, uncertainty in the zero-point determination <0.03 mag; 2 = observation obtained in photometric conditions, uncertainty in the zero-point determination 0.03–0.05 mag; 6 = observation obtained in non photometric conditions, uncertainty in the zero-point determination <0.03 mag; 7 = observation obtained in non photometric conditions, uncertainty in the zero-point determination 0.03–0.06

mag.
Second digit = Image quality code: 0 = image is OK; 1 = small amount of contamination from nearby stars or other galaxies; 2 = significant amount of contamination from nearby stars or other galaxies; 3 = iterative subtraction of the contaminating object required; 4 = flat-fielding of sub-standard quality, due to scattered light from a nearby bright star.
Third digit = Profile code: 1 = $r^{1/4}$ fit good at all radii; 2 = $r^{1/4}$ fit acceptable at all radii; 3 = $r^{1/4}$ fit good only in the core of the galaxy; 4 = the $r^{1/4}$ fit does not provide an acceptable description of the observed photometric profile.
If an asterisk appears in this column, special comments on the object are included at the foot of the table.

A small subset of these data has already been published in Paper I, limited to galaxies in the Coma and A2634 clusters. Since then, a few galaxies have been reobserved, and the data combined to obtain new measurements of the relevant photometric parameters. The data presented here therefore supersede that previous report.

## 6. Internal and external comparison

Repeated observations of the same galaxies provide an opportunity to evaluate the internal consistency of the photometric measurements. In total, repeated observations of 71 galaxies are available. The results of the comparison of effective radius, effective surface brightness, and total magnitude are presented in Figure 2, and they are listed in Table 4. Also listed in this table are the mean statistical uncertainties associated with the derivation of those parameters, multiplied by a $\sqrt{2}$ factor to allow a direct comparison with the rms scatter in the observations (assuming equal error contributions to the rms scatter). Good agreement is found between the separate measurements, with only few isolated significant discrepancies. These are generally due to the uncertainties introduced by the contamination from other nearby objects in the field, as discussed in section 4.1. There is also good general agreement between the rms scatter derived from the comparison and the estimated statistical uncertainties.

The errors on $r_e$ and $\mu_e$ are highly correlated. Figure 3a shows $\Delta \log R_e$ versus $\Delta\mu_e$ for the 71 pairs of observations. The linear correlation coefficient between $\Delta \log R_e$ and $\Delta\mu_e$ is $R = 0.962$. Because $r_e$ and $\mu_e$ enter the FP via the combination $\log R_e - 0.32\ \mu_e$, the correlated nature of the errors on these two quantities translates into a predicted uncertainty on their combination of 0.013, to be compared with the observed scatter of 0.020 (see Figure 3b). Note however that a reduction of $R$ by 10% (the approximate level of uncertainty on its determination) would translate in an increased predicted uncertainty on $\log R_e - 0.32\ \mu_e$ to 0.025.

No large dataset of I band photometric observations of early-type galaxies is available for an external comparison of our photometric measurements. An indirect test can be however obtained using comparisons with similar measurements presented by Lucey *et al.* (1991), Saglia, Bender &

Dressler (1993b), Jørgensen, Franx & Kjærgaard (1995) for galaxies in the Coma cluster. Since none of these studies used I band for the photometric observations, it is necessary to assume standard colors for E and S0 galaxies, before comparisons can be made. The V band magnitudes from Lucey *et al.* (1991), the B band magnitudes from Saglia *et al.* (1993b), and the Gunn r band magnitudes from Jørgensen *et al.* (1995) have been transformed to I band magnitudes using V–I, B–I, and r–I colors of 1.31, 2.25, and 1.07, respectively (Fukugita *et al.* 1995), without taking into consideration the small differences between the brightest and the faintest objects introduced by the color-magnitude relation of early-type galaxies. Because of this, the expected rms scatter in the true colors of E and S0 galaxies around these mean values is expected to be $\simeq 0.2$ mag.

There are 57 galaxies in common with the sample of Lucey *et al.* (1991), 47 with the sample of Saglia *et al.* (1993b), and 106 with the sample of Jørgensen *et al.* (1995). Table 5 and the panels of Figure 4, 5, and 6 show the results of the comparisons of effective radius, effective surface brightness, and the combination $\log R_e - 0.32\,\mu_e$. In these figures, the difference (us - literature) is plotted vs. the average value we can derive for the various parameters using the two respective measurements. There are significant differences in the determinations of both the effective radius and the effective surface brightness. For example, differences as high as 2 mag in the determination of $\mu_e$, after the color correction described above were applied, are present. However it is possible to show that the main source of these differences lies in the different procedures adopted to perform the $r^{1/4}$ fit, and in particular, in the choice of the portion of the photometric profile used for the fit. In this work, the fit was extended to an outer radius chosen on the basis of the shape of the photometric profile: for profiles that do not follow the $r^{1/4}$ relation at all radii, only the core of the galaxy was fitted. If the fit were to have been performed using all the points in the photometric profile, the fitted profile would have a different slope, and both the effective radius and the effective surface brightness would have different values. Another possible source of discrepancy is the choice of the inner radius from where to start the $r^{1/4}$ fit. In this work, this radius was chosen to be twice the radius of the seeing disk. A different choice would likewise lead to a fitted profile with a somewhat different slope, especially for objects with small effective radius.

To quantify this effect, we have reanalyzed the galaxies that show a discrepancy $|\Delta\mu_e| > 1$ mag in Figure 4 and 6 (a total of 20 galaxies). Considering these objects only, we observe differences between our measurements and those taken from the literature of $\Delta \log R_e = 0.48 \pm 0.33$ and $\Delta\mu_e = 1.46 \pm 1.13$, respectively. We have then redetermined $r_e$ and $\mu_e$ for all these galaxies without using the $r^{1/4}$ fit. To do so, we measured on the observed photometric profile the radius that includes half of the total galaxy flux (as derived from the total magnitude, which, in turn, was obtained extrapolating to infinity the outer parts of the photometric profile), and the corresponding average surface brightness. The values of $r_e$ and $\mu_e$ determined using this procedure are in much better agreement with those published by Saglia *et al.* (1993b), and by Jørgensen *et al.* (1995): the new differences between our modified measurements and those taken from the literature are $\Delta \log R_e = 0.063 \pm 0.084$ and $\Delta\mu_e = 0.086 \pm 0.29$, respectively. To help visualize the extent of this problem with different fitting techniques, the panels of Figure 4, 5, and 6 show with filled symbols the galaxies whose photometric profiles follow the $r^{1/4}$ relation at all radii, and with unfilled symbols those galaxies that do not. It is clear that the largest discrepancies are mostly associated with the latter objects.

As we have shown, the observed differences in $\log R_e$ and $\mu_e$ originate from differences in the $r^{1/4}$ fit. As a result there is a correlation between $\Delta \log R_e$ and $\Delta\mu_e$ that is completely analogous to the correlation shown by the errors in $\log R_e$ and $\mu_e$. Therefore, despite the large differences in the two separate values of $\log R_e$ and $\mu_e$, we observe an excellent agreement in the comparison of the combinations $\log R_e - 0.32\ \mu_e$. It is therefore possible to say that these external comparisons show good overall agreement, and establish the good quality of the photometric measurements presented in this work, as well as those presented in the comparison samples.

We would like to thank Gary Wegner, Shoko Sakai, and Bob Barr for their help with the MDM observations, and Bill Schoening for his technical support during the various observing runs at Kitt Peak. This research has made use of the NASA/IPAC Extragalactic Database (NED) which is operated by the Jet Propulsion Laboratory, California Institute of Technology, under contract with the National Aereonautics and Space Administration. This research is part of the Ph.D. Thesis of MS, and is supported by the NSF grants AST94–20505 and AST96–17069 to RG and AST95–28860 to MPH.

## REFERENCES

Bothun, G.D., Geller, M.J., Beers, T.C., & Huchra, J.P. 1983, ApJ, 268, 47

Burstein, D., & Heiles, C. 1978, ApJ, 225, 40

David, L.P., Slyz, A., Jones, C., Forman, W., Vrtilek, S.D., & Arnaud, K.A. 1993, ApJ, 412, 479

de Vaucouleurs, G. 1948, Ann. Astrophys., 11, 247

de Vaucouleurs, G., de Vaucouleurs, A., Corwin, H.G., Buta, R., Paturel, G., & Fouqué, P. 1991, "Third Reference Catalogue of Bright Galaxies" (New York: Springer) (RC3)

Djorgovski, S.G., & Davis, M. 1987, ApJ, 313, 59

Djorgovski, S.G., De Carvalho, R.R., & Han, M.S. 1988, in "The Extragalactic Distance Scale", ed. S. van den Bergh & J. Pritchet, p. 329

Dressler, A. 1980, ApJS, 42, 565

Dressler, A., Lynden-Bell, D., Burstein, D., Davies, R.L., Faber, S.M., Terlevich, R.J., & Wegner, G. 1987, ApJ, 313, 42

Edge, A.C., & Stewart, G.C. 1991, MNRAS, 252, 428

Forman, W., & Jones, C. 1982, ARA&A, 20, 547

Fukugita, M., Shimasaku, K., & Ichikawa, T. 1995, PASP, 107, 945

Gavazzi, G., Randone, I., & Branchini, E. 1995, ApJ, 438, 590

Giovanelli, R., & Haynes, M.P. 1985, AJ, 90, 2445

Giovanelli, R., Haynes, M.P., Herter, T., Vogt, N.P., da Costa, L.N., Freudling, W., Salzer, J.J., & Wegner, G. 1997a, AJ, 113, 22 (G97a)

Giovanelli, R., Haynes, M.P., Herter, T., Vogt, N.P., da Costa, L.N., Freudling, W., Salzer, J.J., & Wegner, G. 1997b, AJ, 113, 53 (G97b)

Guzmán, R., Lucey, J.R., Carter, D., & Terlevich, R.J. 1992, MNRAS, 257, 187

Guzmán, R., Lucey, J.R., Bower, R.G., 1993, MNRAS, 265, 731

Haynes, M.P., & Giovanelli, R., 1984, AJ, 89, 758

Jørgensen, I., Franx, M. & Kjærgaard, P. 1995, MNRAS, 273, 1097

Jørgensen, I., Franx, M., & Kjærgaard, P. 1996, MNRAS, 280, 167

Kaiser, N. 1987, MNRAS, 227, 1

Kogut, A., et al. 1993, ApJ, 419, 1

Landolt, A.U. 1992, AJ, 104, 340

Lucey, J.R., Guzmán, R., Carter, D., & Terlevich, R.J. 1991, MNRAS, 253, 584

Magri, C., Haynes, M.P., Forman, W., Jones, C., & Giovanelli, R. 1988, ApJ, 333, 136

Nilson, P. 1973, "Uppsala General Catalogue of Galaxies" (Uppsala Astron. Obs. Ann., Vol. 6) (UGC)

Pahre, M.A., & Djorgovski, S.G., 1997, in "The Nature of Elliptical Galaxies, Proceedings of the Second Stromlo Symposium", ASP Conf. Series 116, eds. M. Arnaboldi, G. S. Da Costa, and P. Saha, p. 154

Pinkney, J., Rhee, G., Burns. J.O., Hill, J.M., Oegerle, W.M., Batuski, D., & Hintzen, P. 1993, ApJ, 416, 36

Regös, E., & Geller, M.J. 1989, AJ, 98, 755

Renzini, A., & Ciotti, L., 1993, ApJ, 416, L49

Saglia, R., Bertschinger, E., Baggley, G., Burstein, D., Colless, M., Davies, R.L., McMahan, R.K., & Wegner, G. 1993a, MNRAS, 264, 961

Saglia, R.P., Bender, R., & Dressler, A. 1993b,A&A, 279, 75

Sakai, S., Giovanelli, R., & Wegner, G. 1994, AJ, 108, 33

Sarazin, C.L., 1988, "X-ray emission from clusters of galaxies" (Cambridge: Cambridge University Press)

Schindler, S., & Prieto, M.A., 1997, A&A, 327, 37

Schlegel, D.J., Finkbeiner, D.P., & Davis, M., 1998, ApJ, 500, 525

Schroeder, A., 1996, PhD Thesis, Univ. of Basel

Scodeggio, M., Solanes, J.M., Giovanelli, R., & Haynes, M.P. 1995, ApJ, 444, 41

Scodeggio, M., Giovanelli, R., & Haynes, M.P. 1997a, AJ, 113, 101 (Paper I)

Scodeggio, M., Giovanelli, R., & Haynes, M.P. 1997b, AJ, 113, 2087 (Paper II)

Scodeggio, M., Giovanelli, R., & Haynes, M.P. 1998a, submitted to AJ

Scodeggio, M., Giovanelli, R., & Haynes, M.P. 1998b, in preparation

Tully, R.B., & Fisher, J.R. 1977, A&A, 54, 661

van Dokkum, P.G., & Franx, M. 1996, MNRAS, 281, 985

van Haarlem, M.P. 1992, PhD Thesis, Univ. of Leiden

Zabludoff, A.I., Huchra, J.P., & Geller, M.J. 1990, ApJS, 74, 1

Zwicky, F., Herzog, E., Wild, P., Karpowicz, M., & Kowal, C. 1961–1968, "Catalogue of Galaxies and Clusters of Galaxies" (Pasadena: California Institute of Technology)

Table 2: Imaging observing runs

| | Run 1 | Run 2, 4–8 | Run 3 |
|---|---|---|---|
| Telescope | MDM 1.3m | KPNO 0.9m | MDM 1.3m |
| CCD | Loral2048 (Wilbur) | T2KA | Tek1024 (Charlotte) |
| Pixels | 1024 x 1024 | 2048 x 2048 | 1024 x 1024 |
| Read-out noise | 6.0 $e^-$ | 4.0 $e^-$ | 4.8 $e^-$ |
| Gain | 1.9 $e^-$/DU | 3.2 $e^-$/DU | 3.45 $e^-$/DU |
| Pixel scale | 0.63 ″/pixel | 0.68 ″/pixel | 0.51 ″/pixel |
| Field of view | 11 x 11 arcmin | 23 x 23 arcmin | 9 x 9 arcmin |

| | Run 1 | Run 2 | Run 3 | Run 4 |
|---|---|---|---|---|
| Dates | Sep. 23-25 1992[a] | Aug. 18-20 1993[b] | Sep. 8-9 1993[a] | Apr. 14-19 1994 |
| Photometric nights | 3 | 0 | 2 | 3 |
| Marginal nights | 0 | 3 | 0 | 1 |
| Nr. of galaxies | 10 | 78 | 6 | 322 |

| | Run 5 | Run 6 | Run 7 | Run 8 |
|---|---|---|---|---|
| Dates | Aug. 31 - Sep. 6 1994 | Oct. 8 1994[a] | Mar. 6 1995[a] | Sep. 24 - Oct. 1 1995 |
| Photometric nights | 3 | 1 | 0 | 2 |
| Marginal nights | 1 | 0 | 1 | 2 |
| Nr. of galaxies | 223 | 16 | 5 | 47 |

[a]Observing run mainly dedicated to a different project; only a small portion of telescope time dedicated to this project.

[b]Service observing by KPNO personnel.

Table 4. Imaging data quality: internal comparison

| Parameter | $N_{gal}$ | mean difference | rms scatter | mean uncertainty |
|---|---|---|---|---|
| $\log r_e$ | 71 | -0.003 | 0.044 | 0.038 |
| $\mu_e$ | 71 | -0.001 | 0.131 | 0.113 |
| $m_{tot}$ | 71 | 0.071 | 0.087 | 0.084 |
| $\log r_e - 0.32\mu_e$ | 71 | 0.001 | 0.020 | 0.013 |

Table 5. Imaging data quality: External Comparison

| Parameter | $N_{gal}$ | mean difference | rms scatter |
|---|---|---|---|
| | | Saglia et al. (B band) | |
| $\log r_e$ | 47 | 0.158 | 0.240 |
| $\mu_e$ | 47 | 0.365 | 0.813 |
| $\log r_e - 0.32\mu_e$ | 47 | 0.034 | 0.043 |
| | | Lucey et al. (V band) | |
| $\log r_e$ | 57 | 0.030 | 0.100 |
| $\mu_e$ | 57 | -0.100 | 0.353 |
| $\log r_e - 0.32\mu_e$ | 57 | 0.060 | 0.030 |
| | | Jørgensen et al. (r band) | |
| $\log r_e$ | 106 | 0.173 | 0.248 |
| $\mu_e$ | 106 | 0.438 | 0.741 |
| $\log r_e - 0.32\mu_e$ | 106 | 0.031 | 0.038 |

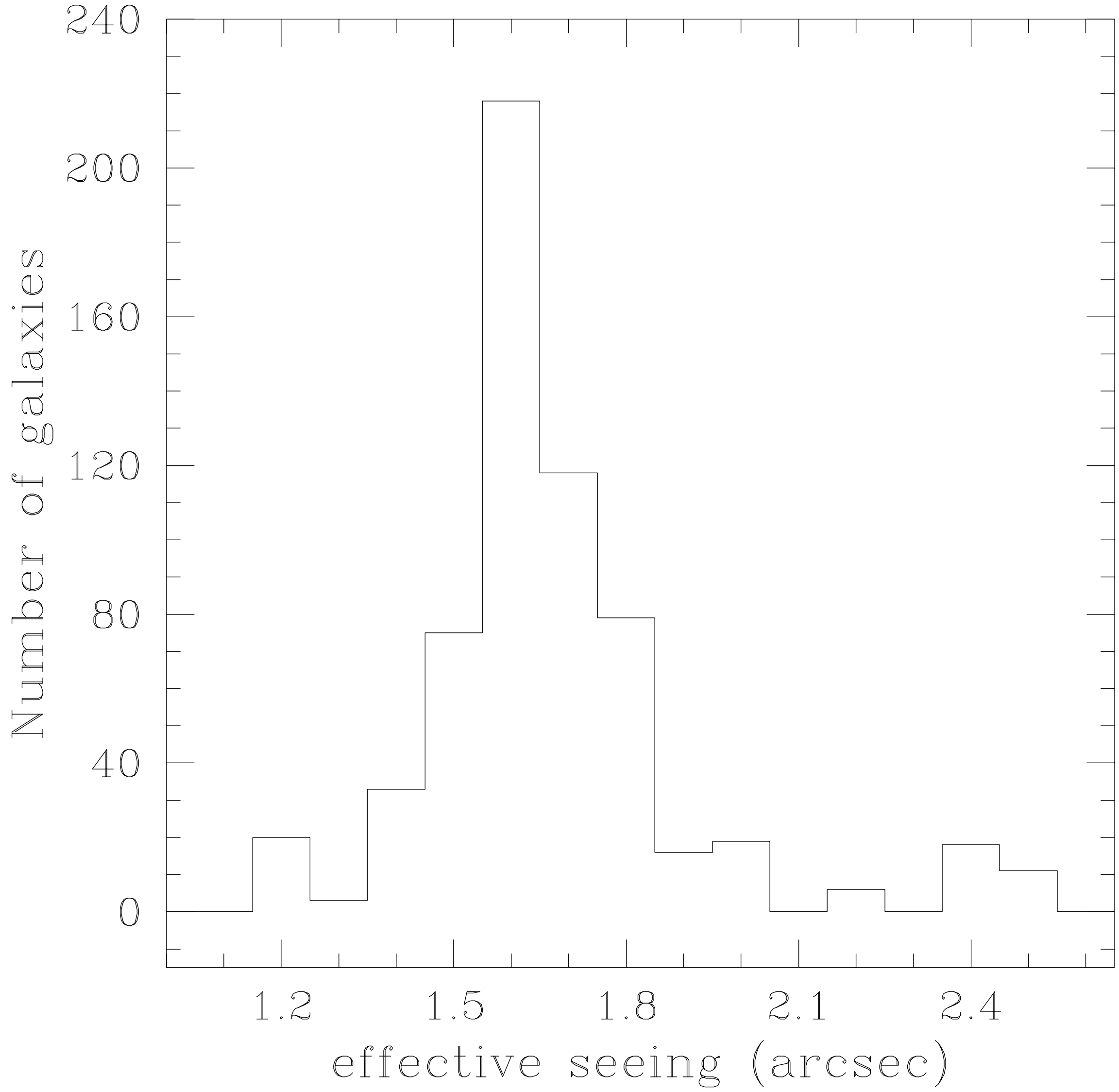


Fig. 1.— The distribution of effective seeing for the galaxy observations. The pixel size of 0.68 arcsec. limits this effective seeing to be no smaller than ≃1.2 arcsec.

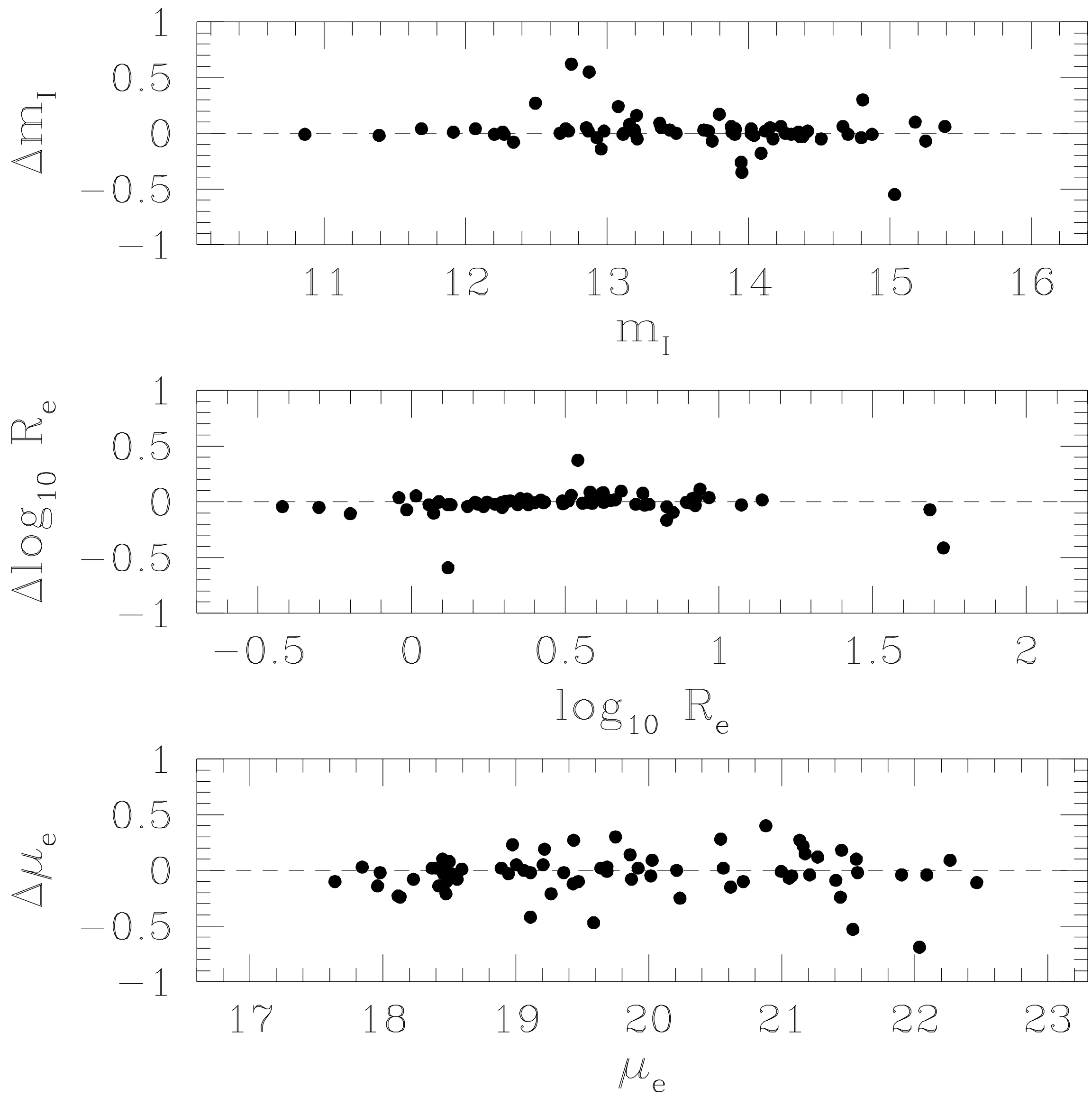


Fig. 2.— Internal comparison of the global photometric parameters. $\Delta m_I$, $\Delta log_{10} R_e$, and $\Delta \mu_e$ are the differences between the values of the total magnitude, effective radius, and effective surface brightness obtained from repeated observations of 71 galaxies. They are plotted as a function of the mean value of the relative parameter, obtained combining the different measurements.

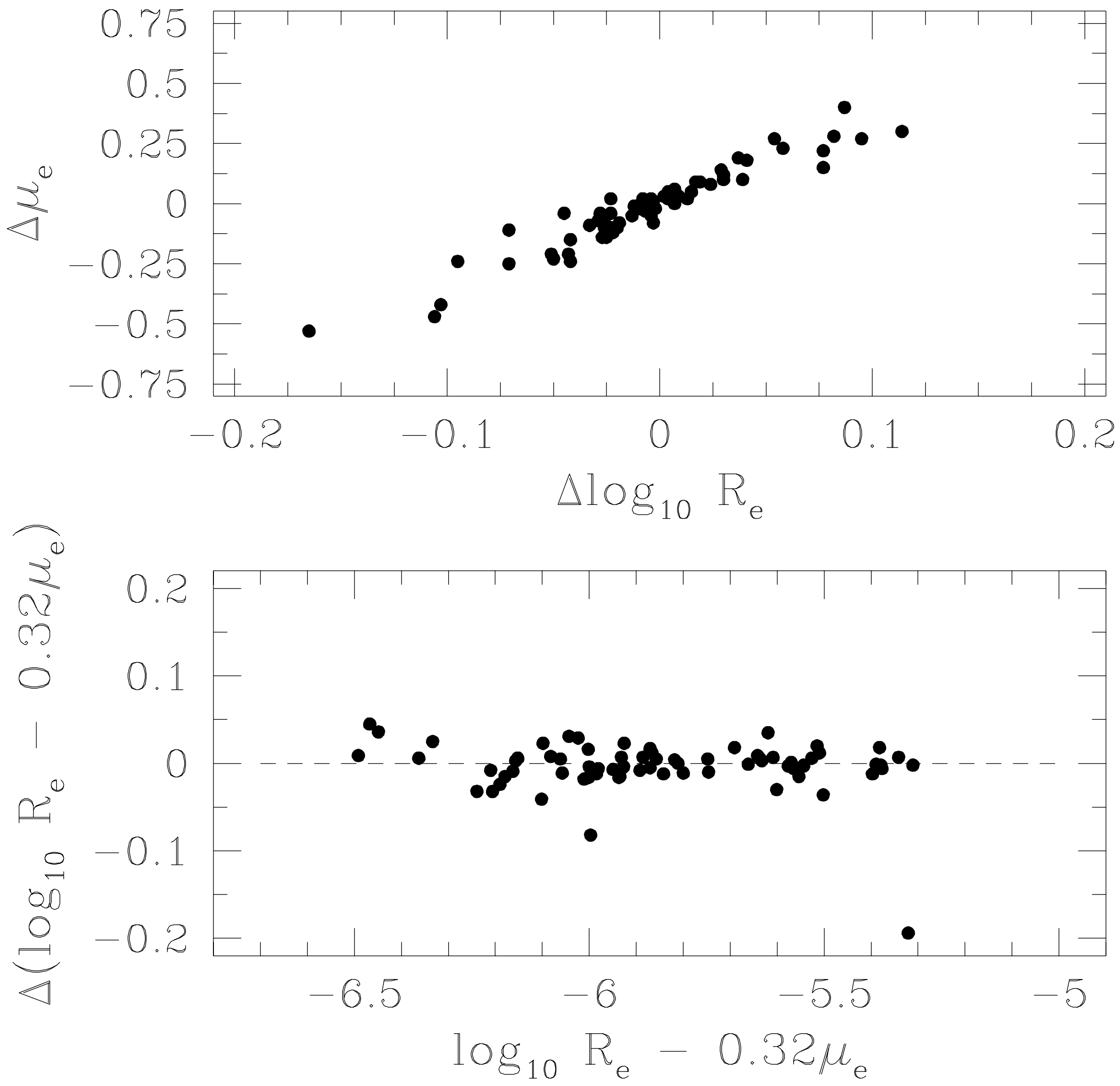


Fig. 3.— (a) The correlation of the errors in $\log r_e$ and $\mu_e$. The figure shows the differences measured from repeated observations. The linear correlation coefficient for this data-set is 0.962. (b) Internal comparison of the combination $\log r_e - 0.32\ \mu_e$, which is the combination that enters in the FP relation. As in Fig.2, the difference derived from repeated observations is plotted against the mean value of the parameter.

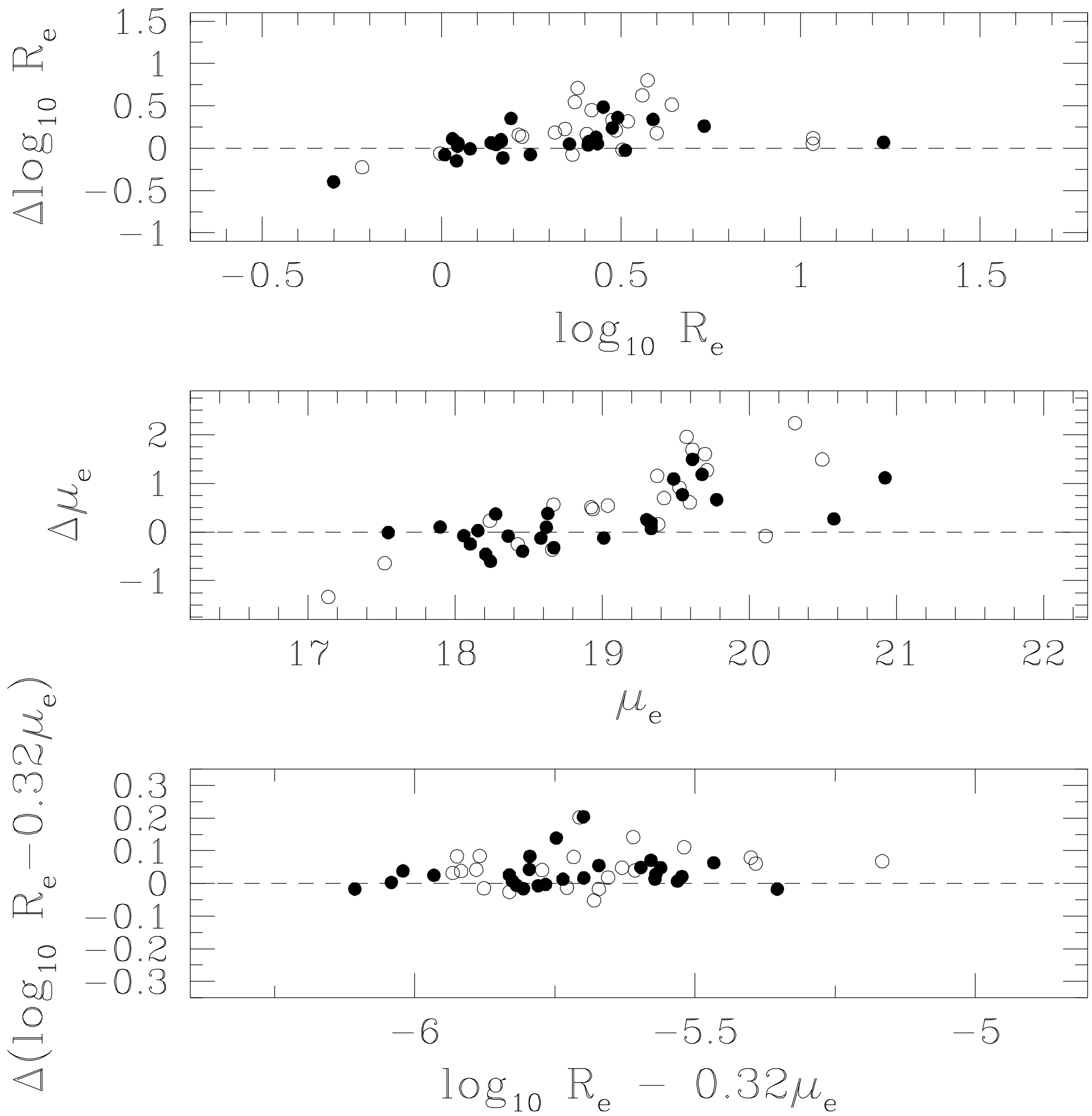


Fig. 4.— External comparison of the global photometric parameters for galaxies in the Coma cluster with the B band data from Saglia et al. B magnitudes were converted to I magnitudes for the comparison, assuming a fixed B-I color (see text). Filled symbols identify the galaxies whose photometric profile follows the $r^{1/4}$ relation at all radii, while empty symbols identify those galaxies that deviate significantly from such a profile. The differences (us - Saglia) are plotted against the mean value of the different parameters, obtained combining the two measurements.

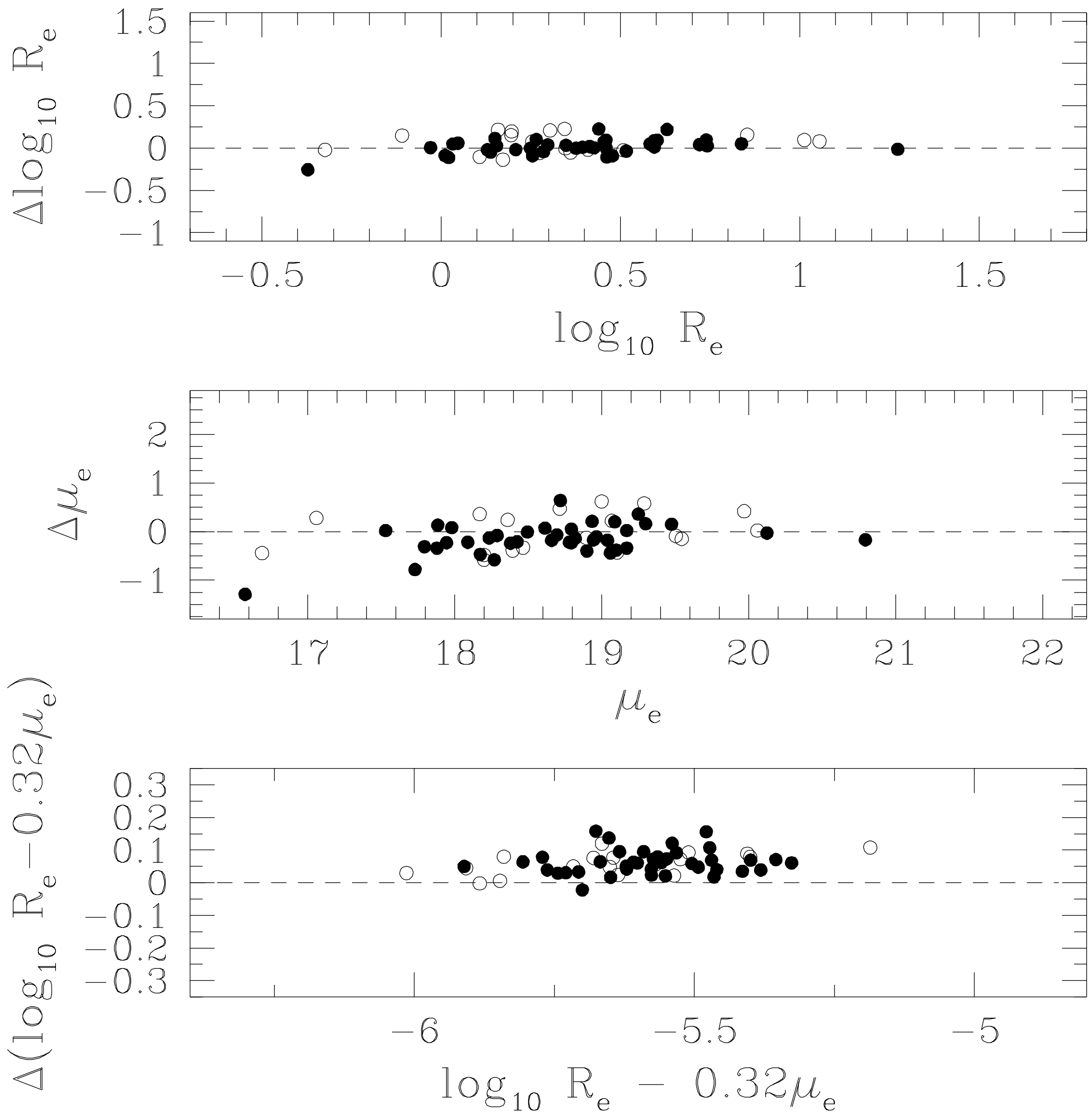


Fig. 5.— External comparison of the global photometric parameters for galaxies in the Coma cluster with the V band data from Lucey et al. V magnitudes were converted to I magnitudes for the comparison, assuming a fixed V-I color (see text). Filled symbols identify the galaxies whose photometric profile follows the $r^{1/4}$ relation at all radii, while empty symbols identify those galaxies that deviate significantly from such a profile. As in the previos figure, differences (us - Lucey) are plotted against the mean value of the different parameters.

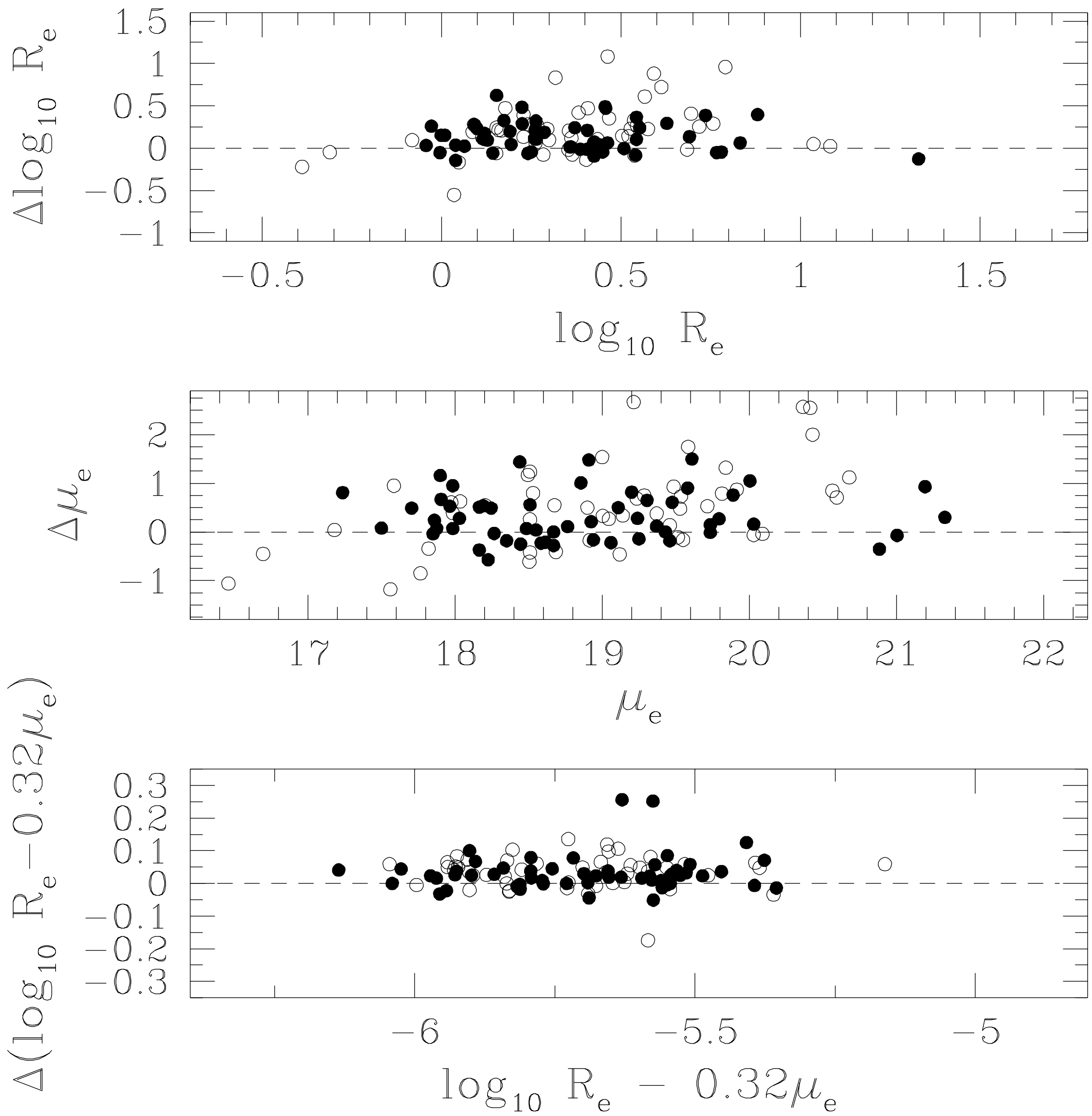


Fig. 6.— External comparison of the global photometric parameters for galaxies in the Coma cluster with the r band data of Jørgensen et al. r magnitudes were converted to I magnitudes for the comparison, assuming a fixed r-I color (see text). Filled symbols identify the galaxies whose photometric profile follows the $r^{1/4}$ relation at all radii, while empty symbols identify those galaxies that deviate significantly from such a profile. As in the previos figure, differences (us - Jørgensen) are plotted against the mean value of the different parameters.